Int. J. Adv. Eng. Pure Sci. 2023, 35(3): 331-337
DOI: 10.7240/jeps.1257560

RESEARCH ARTICLE / ARAŞTIRMA MAKALESİ

Effects of Flow Parameters on Heat Transfer and Temperature Distribution of a Thermoelectric Module

Furkan KILIÇ [1], **Enes KILINÇ** [1]

[1]*Karabük University, Faculty of Engineering, Department of Mechanical Engineering, Karabük, Türkiye*

Abstract
The effects of the hot air inlet velocity and hot air inlet temperature on the hot side temperature, the temperature difference between the hot and cold sides, and the heat transfer rate on the hot side of a thermoelectric module (TEM) were investigated by computational fluid dynamics (CFD) analyzes. CFD model is constituted as hot and cold air will flow on both sides of the TEM. During the analyzes, hot and cold air inlet velocities are varied between 1 m/s and 15 m/s, while hot air inlet temperature is altered between 400 °C and 800 °C. Simultaneously, cold air inlet temperature is kept constant at 25 °C. As a result of CFD analysis, the maximum hot side temperature, the temperature difference between the hot and cold sides, and the average heat transfer rate on the hot side of the TEM are found to be 274.9 °C, 70.4 °C, and 33.8 W, respectively, at 15 m/s of hot air inlet velocity. Besides, the maximum hot side temperature, the temperature difference between the hot and cold sides, and the average heat transfer rate on the hot side of the TEM are determined to be 432.8 °C, 114.9 °C, and 55.1 W, respectively, for 800 °C of hot air inlet temperature at 15 m/s of hot air inlet velocity. As a result, increasing the hot air inlet velocity and inlet temperature increases the hot side temperature, the temperature difference between the hot and cold sides, and the heat transfer rate on the hot side of the TEM.
Keywords: Thermoelectrics, thermoelectric power generation, heat transfer, temperature distribution, CFD.

Öz
Bu çalışmada, sıcak hava giriş hızı ve sıcak hava giriş sıcaklığının bir termoelektrik modülün (TEM) sıcak yüzey sıcaklığına, sıcak ve soğuk yüzeyler arasındaki sıcaklık farkına ve sıcak yüzeydeki ısı transfer hızına etkisi hesaplamalı akışkanlar dinamiği (HAD) analizleri ile incelenmiştir. HAD analizleri sonucunda TEM'in maksimum sıcak taraf sıcaklığı, sıcak ve soğuk yüzey arasındaki sıcaklık farkı ve sıcak yüzeydeki ortalama ısı transfer hızı 15 m/s sıcak hava giriş hızında sırasıyla 274,9 °C, 70,4 °C ve 33,8 W olarak bulunmuştur. Diğer taraftan, TEM'in maksimum sıcak yüzey sıcaklığı, sıcak ve soğuk yüzeyler arasındaki sıcaklık farkı ve sıcak yüzeydeki ortalama ısı transfer hızı 15 m/s sıcak hava giriş hızı ve 800 °C sıcak hava giriş sıcaklığı için sırasıyla 432,8 °C, 114,9 °C ve 55,1 W olarak belirlenmiştir. Sonuç olarak, sıcak hava giriş hızının ve giriş sıcaklığının artması, TEM'in sıcak yüzey sıcaklığını, sıcak ve soğuk yüzeyler arasındaki sıcaklık farkını ve sıcak yüzeydeki ısı transfer hızını artırmıştır.
Anahtar Kelimeler: Termoelektrik, Termoelektrik Güç Üretimi, Isı Transferi, Sıcaklık Dağılımı, CFD.

I. INTRODUCTION

Thermoelectric technology has been used in laboratorial and industrial engineering applications in thermoelectric modules (TEMs) and thermoelectric generators. Recently, TEMs have been widely used as coolers for cooling applications and electricity generators on the closure side of the photovoltaic cells to decrease the temperature [1–3]. On the other hand, they can be used as alternative electricity generators utilizing available waste heat from factories, automobiles, etc., due to the thermoelectric effect [4]. Currently, researchers declare analytical studies focusing on the application of TEMs in the exhaust system of an automobile to retrieve the exhaust gas waste heat [5]. Other heat sources, including waste heat, can also generate a temperature difference between the hot and cold sides of the TEMs (ΔT) to produce electricity [6]. Other studies suggest that TEMs formed in different designs have a higher consciousness of radiation heat in industrial furnace applications [7].

A three-dimensional model of the TEM can be created by computational fluid dynamics (CFD) to investigate and optimize the temperature distribution on both sides and the power generation performance of the TEM [8]. The finite difference method model covers Seebeck, Joule, and Thomson effects equations, including Fourier's law and temperature-dependent properties. Also, the model structure gives numerical analysis higher accuracy, even in more complicated designs [9].

Corresponding Author: Enes KILINÇ, **Tel:** +90 532 3401163, **e-posta:** eneskilinc@karabuk.edu.tr
Submitted: 28.02.2023, **Revised:** 03.07.2023, **Accepted:** 03.08.2023

In TEM applications, different fluids can pass through both sides of the TEM. The type, velocity, and other parameters of the fluid affect the temperature distributions on both sides, heat transfer, and, therefore, the electrical power to be obtained from the TEM. Bell mentioned the need to connect TEMs with fluid flows flowing in opposite directions (counter-current flow) to obtain wider temperature ranges in his series work [10]. In their study, Temizer and Ilkilic investigated the exhaust gas flow and temperatures of the internal combustion engine at different speeds and loads and the different fluid flow directions. As a result, the counter-flow direction can increase the heat transfer, thus TE power generation from the exhaust gas heat using the Ansys 12.0 Fluent software [11]. As a result of the analysis, the water temperature increased along the surface, and the cooling efficiency decreased. Although there is a tendency to decrease the pressure and flow values of the exhaust gas at a certain distance when it enters the TEM system, there was not much change, and there was no loss compared to the inlet. In their study, He et al. examined different flow types on both sides of the TEM [12]. Output powers were analyzed according to
yielding greater thermoelectric output power than the co-flow direction.

In this study, the hot side temperature (T_{hs}), ΔT, and the heat transfer rate on the hot side of the TEM ($\dot{Q}_h$) were investigated by passing hot and cold air over both sides of the TEM, designed in ANSYS DesignModeler software. Flow analyses were performed using CFD analysis on ANSYS Fluent software. Hot air and cold air are modeled to flow as counter-flow to increase ΔT and $\dot{Q}_h$. Hot air inlet velocity (V_{hi}) and cold air inlet velocity (V_{ci}) were varied as 1 m/s, 3 m/s, 5 m/s, 10 m/s, and 15 m/s by keeping the hot air inlet temperature (T_{hi}) at 500 °C and the cold air inlet temperature (T_{ci}) at 25 °C. By keeping V_{hi} at 15 m/s and T_{ci} at 25 °C, T_{hi} ranged from 400 °C, 500 °C, 600 °C, 700 °C, and 800 °C. Effects of V_{hi} and the T_{hi} on the temperature distribution and $\dot{Q}_h$ of the TEM were investigated.

II. METHODOLOGY

In this study, CFD analyses of a TEM composed of 8 pairs of p- and n-type TE legs with circular cross-sections were used to evaluate the temperature distribution and $\dot{Q}_h$ on the TEM. The CFD analysis of the TEM was performed on Ansys Fluent software. Air was used as the fluid for both surfaces of the TEM in the analysis. During the CFD analyses, the temperature distribution on both sides and $\dot{Q}_h$ of the TEM were investigated at different V_{hi} and T_{hi}. In the analyses, the TEM was designed in ANSYS DesignModeler. Appropriate mesh structure was obtained for the analysis, and boundary conditions were determined by defining material and fluid properties in Ansys Fluent. The effects of V_{hi} and T_{hi} on the temperature distribution and $\dot{Q}_h$ of the TEM were investigated as a result of the analysis.

The TEM model was constituted as the legs of the TEM are connected in series for electrical connection and parallel for the heat transfer. The dimensions of both legs were designed to be Ø8x5 mm, and the distance between the legs was designed as 3 mm. In the model, the legs were placed between 2 pieces of alumina plates with 50x50x1 mm dimensions. The meshing of the TEM model performed using the finite volume method is shown in **Figure 1**.

For the flow analyses, CFD model was constituted as hot and cold air would flow on both sides of the TEM. Hot and cold air enclosures were designed using ANSYS DesignModeler software for both sides of the TEM. After generating hot and cold air enclosures, the designed TEM model was transferred to ANSYS Fluent software. The inlet and outlet of the hot and cold flows were specified as there will be a counter-current flow to increase ΔT and $\dot{Q}_h$. Walls of the hot and cold air enclosures and lateral surfaces of the TEM were considered adiabatic in the model. The no-slip condition was applied for the fluids flowing on both sides of the TEM. In the solution setup, V_{hi} and V_{ci} of 1 m/s, 3 m/s, 5 m/s, 10 m/s, and 15 m/s, and T_{hi} of 400 °C, 500 °C, 600 °C, 700 °C, and 800 °C were specified as the inlet boundary conditions. Simultaneously, cold air inlet temperature was kept constant at 25 °C. The ambient temperature and the convection heat transfer coefficient for the outer surfaces were defined as 25 °C and 10 W/m^{2}K, respectively. Moreover, the thermal and thermoelectric properties of alumina plates, silver conductors, p- and n-type legs, and the fluid properties of air flowing on both sides of the TEM were specified.

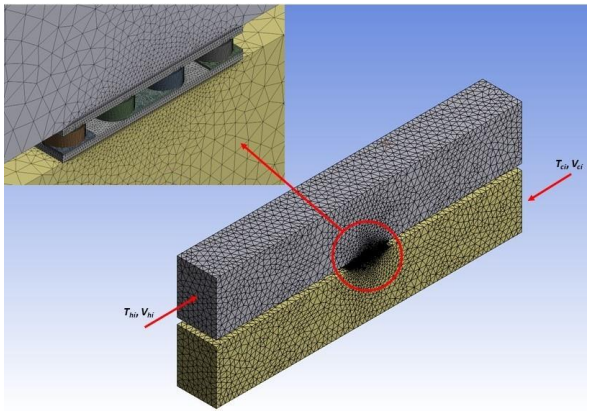

Figure 1. TEM model for the CFD analyses.

Mesh number and mesh quality are important parameters in CFD analyses to get results closer to reality. The adequate number of mesh nodes and elements suitable for the TEM determines the quality of the meshing process. Since the software uses a lot of CPU in the computer, mesh optimization is very important in terms of time-saving. In this respect, two different body sizing were defined in the bottom tab of the meshing process, and different meshing properties were defined according to the dimensions of the TEM's parts. The first type of body sizing was applied for the silver conductors and the legs in the TEM, while the second type was applied for the alumina plates. The average element sizes for the sections where the first and second types of body sizing were applied were defined as 0.25 mm and 0.5 mm, respectively. The average element size of the remaining meshing of the enclosure sections was 5 mm. As a result, number of elements was optimized at 2,915,567 elements using tetrahedral and hexahedral elements. Lastly, the analyses were optimized in 500 iterations, and the results were obtained.

III. RESULTS AND DISCUSSION

3.1. Effect of the Hot Air Inlet Velocity on the Temperature Distribution of the TEM

CFD analyses were carried out to determine the temperature distributions on both sides and through the TEM at different hot air inlet velocities. T_{hi} and T_{ci} of the TEM were taken constantly at 500 °C and 25 °C, respectively, while modifying V_{hi}. V_{hi} was altered as 1 m/s, 3 m/s, 5 m/s, 10 m/s, and 15 m/s. As a result of the analyses, the temperature distributions on both sides and the temperature distribution through the TEM are shown in **Figure 2** to **Figure 6** for V_{hi} of 1 m/s, 3 m/s, 5 m/s, 10 m/s, and 15 m/s, respectively.

Obtaining the results, the temperature drops between the inlet and outlet regions of both sides of the TEM were observed. Increasing V_{hi} increases T_{hs}, cold side temperature (T_{cs}), and ΔT between both sides of the TEM, and the temperature distributions show similar characteristics at all V_{hi}.

When **Figure 2** is examined, the maximum T_{hs} and T_{cs} of the TEM are obtained as 122.7 °C and 114.7 °C, while the maximum temperature through the TEM is found to be 122.3 °C for 1 m/s of V_{hi}. According to **Figure 3**, when the V_{hi} increases to 3 m/s, the maximum T_{hs} and T_{cs} of the TEM increase similarly to 186.4 °C and 165.7 °C, respectively, while the maximum temperature through the TEM increases to 184.2 °C. When the V_{hi} increases to 5 m/s, the TEM's maximum T_{hs} and T_{cs} are realized as 214.6 °C and 183.9 °C, respectively. The maximum temperature through the TEM is 211.3 °C (**Figure 4**). **Figure 5** illustrates the temperature distributions on both sides and through the TEM for 10 m/s of V_{hi}. According to the figure, the maximum T_{hs} and T_{cs} of the TEM are found to be 252.8 °C and 200.5 °C, respectively, while the maximum temperature through the TEM is obtained as 247.1 °C. Finally, when **Figure 6** is inspected, the TEM's maximum T_{hs} and T_{cs} are acquired as 274.9 °C and 204.5 °C, while the maximum temperature through the TEM is 266.9 °C for 15 m/s of V_{hi}. According to these results, the increase in T_{hs} of the TEM with the increase in the V_{hi} can be attributed to the increase in the Re number, which yields an increase in the Nu number and the convection heat transfer coefficient.

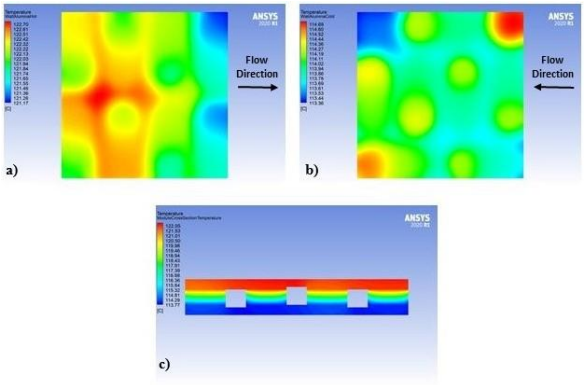

Figure 2. Temperature distributions for 1 m/s of V_{hi}: a) on the hot side of the TEM, b) on the cold side of the TEM, and c) through the TEM.

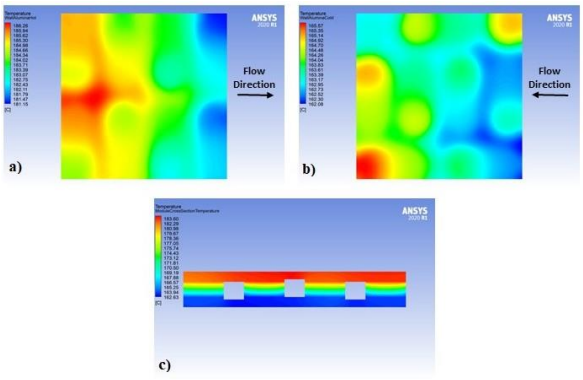

Figure 3. Temperature distributions for 3 m/s of V_{hi}: a) on the hot side of the TEM, b) on the cold side of the TEM, and c) through the TEM.

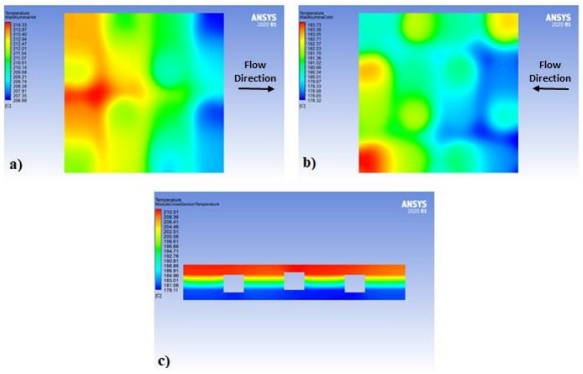

Figure 4. Temperature distributions for 5 m/s of V_{hi}: a) on the hot side of the TEM, b) on the cold side of the TEM, and c) through the TEM.

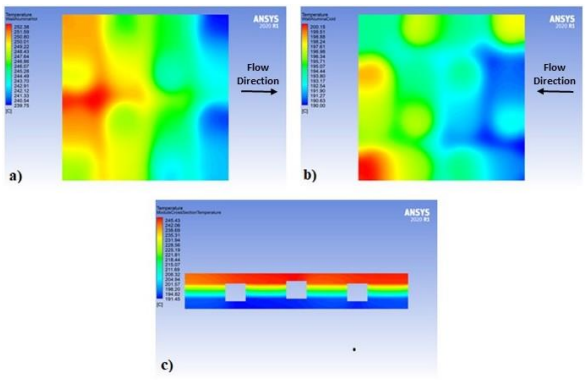

Figure 5. Temperature distributions for 10 m/s of V_{hi}: a) on the hot side of the TEM, b) on the cold side of the TEM, and c) through the TEM.

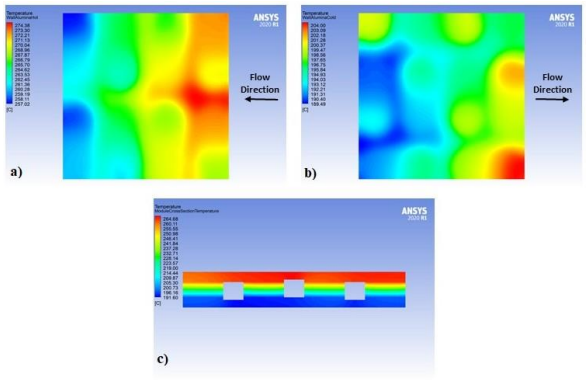

Figure 6. Temperature distributions for 15 m/s of V_{hi}: a) on the hot side of the TEM, b) on the cold side of the TEM, and c) through the TEM.

According to the temperature distributions, it has been analyzed that ΔT of the TEM increase with the increase in V_{hi}. This increase results in ΔT of 8.0 °C, 20.7 °C, 30.7 °C, 52.3 °C, and 70.4 °C for 1 m/s, 3 m/s, 5 m/s, 10 m/s, and 15 m/s of V_{hi}, respectively, under constant T_{hi} and T_{ci}. The TEM's T_{hs} *and* T_{cs} for the V_{hi} are given in **Figure 7**. When the temperature distributions are further investigated, it seems that temperature distributions on both sides of the TEM are not homogeneous. The temperature differences on the hot side are 1.5 °C, 5.1 °C, 7.4 °C, 12.6 °C, and 17.3 °C, where the temperature differences on the cold side are 1.3 °C, 3.4 °C, 5.4 °C, 10.1 °C, and 14.5 °C for 1 m/s, 3 m/s, 5 m/s, 10 m/s, and 15 m/s of V_{hi}, respectively. This difference on the same surface originates from the difference between the conduction heat transfer (occurs between the alumina plate and the silver conductor and between the silver conductor and p- and n-type legs) and the convection heat transfer (occurs between the alumina plate and the ambient air and between p- and n-type legs and the ambient air). In addition, the difference in the thermal conductivity values of the TEM materials (silver conductor and p- and n-type legs) constitutes different values for the conduction heat transfer.

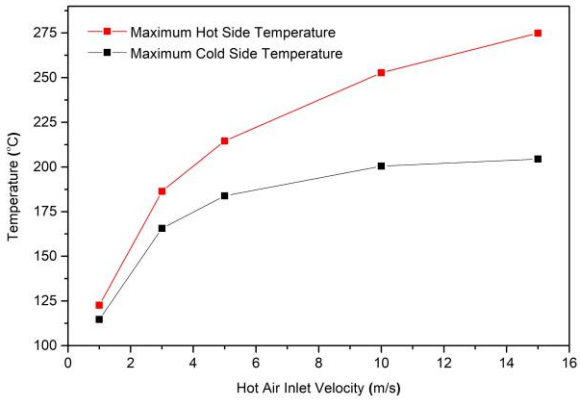

Figure 7. Effect of the V_{hi} on the T_{hs} and T_{cs} of the TEM.

In addition to temperature distributions, the average heat transfer rates on the hot ($\dot{Q}_h$) and cold sides ($\dot{Q}_c$) of the TEM were investigated. According to the results in **Table 1**, the average $\dot{Q}_h$ are found to be 4.6 W, 11.3 W, 16.1 W, 25.6 W, and 33.8 W for 1 m/s, 3 m/s, 5 m/s, 10 m/s, and 15 m/s of V_{hi}, respectively. In addition, the average $\dot{Q}_c$ is analyzed to be 1.8 W, 6.7 W, 10.9 W, 20.0 W, and 28.2 W for 1 m/s, 3 m/s, 5 m/s, 10 m/s, and 15 m/s of V_{hi}, respectively. According to these results, increasing V_{hi} yields an increase in $\dot{Q}_h$ and $\dot{Q}_c$. As expected, the maximum average $\dot{Q}_h$ and $\dot{Q}_c$ resulted in the maximum V_{hi}. The increase in $\dot{Q}_h$ and $\dot{Q}_c$ can be attributed to the increase in the Re number, which yields an increase in the Nu number and the convection heat transfer coefficient.

Table 1. Average $\dot{Q}_h$ and $\dot{Q}_c$ for V_{hi}.

V_{hi} [m/s]	$\dot{Q}_h$ [W]	$\dot{Q}_c$ [W]	T_{hs} [°C]	T_{cs} [°C]	ΔT [°C]
1	4.6	1.8	122.7	114.7	8.0
3	11.3	6.7	186.4	165.7	20.7
5	16.1	10.9	214.6	183.9	30.7
10	25.6	20.0	252.8	200.5	52.3
15	33.8	28.2	274.9	204.5	70.4

3.2. Effect of the Hot Air Inlet Temperature on the Temperature Distribution of the TEM

CFD analyses were carried out to determine the temperature distributions on both sides and through the TEM at different T_{hi}. When the effect of the V_{hi} on the temperature distribution of the TEM was analyzed, it was specified that the maximum T_{hs} and the maximum ΔT were obtained at 15 m/s of the V_{hi}. Accordingly, the V_{hi} of the TEM was kept constant at 15 m/s while modifying T_{hi}. During the analyses, T_{ci} was kept constant at 25 °C, and the T_{hi} were varied to 400 °C, 500 °C, 600 °C, 700 °C, and 800 °C. As a result of the analyses, the temperature distributions on both sides and through the TEM are shown in **Figure 8** to **Figure 12** for the T_{hi} of 400 °C, 500 °C, 600 °C, 700 °C, and 800 °C, respectively.

According to the CFD results, the temperature drops between the inlet and outlet regions of both sides of the TEM were observed. Increasing the T_{hi} increases the T_{hs} and T_{cs} and ΔT of the TEM. As can be seen from the figures, the temperature distributions show similar characteristics at all T_{hi}.

When **Figure 8** is examined, the maximum T_{hs} and T_{cs} of the TEM are obtained as 222.3 °C and 166.7 °C, while the maximum temperature through the TEM is found to be 216.0 °C for 400 °C of T_{hi}. According to **Figure 9**, when the T_{hi} increases to 500 °C, the maximum T_{hs} and T_{cs} of the TEM increase in a similar manner to 274.9 °C and 204.5 °C, respectively, while the maximum temperature through the TEM increases to 266.9 °C. When the T_{hi} increases to 600 °C, the TEM's maximum T_{hs} and T_{cs} are realized as 327.5 °C and 242.3 °C, respectively. The maximum temperature through the TEM is 317.9 °C (**Figure 10**). **Figure 11** illustrates the temperature distributions on both sides and through the TEM for 700 °C of T_{hi}. According to the figure, the maximum T_{hs} and T_{cs} of the TEM are found to be 380.1 °C and 280.0 °C, respectively, while the maximum temperature through the TEM is obtained as 368.8 °C. Finally, when **Figure 12** is inspected, the maximum T_{hs} and T_{cs} of the TEM are acquired as 432.8 °C and 317.8 °C, while the maximum temperature through the TEM is found to be 419.8 °C for 800 °C of T_{hi}. According to these results, the increase in the T_{hs} of the TEM with the increase in the T_{hi} can be attributed to the increase in the ΔT between the hot air and the hot side of the TEM, which yields an increase in the convection heat transfer rate.

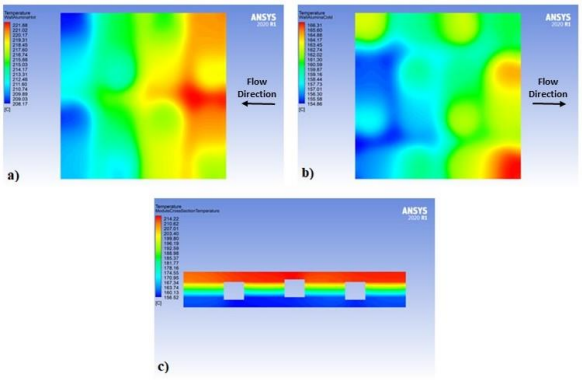

Figure 8. Temperature distributions for 400 °C of T_{hi}: a) on the hot side of the TEM, b) on the cold side of the TEM, and c) through the TEM.

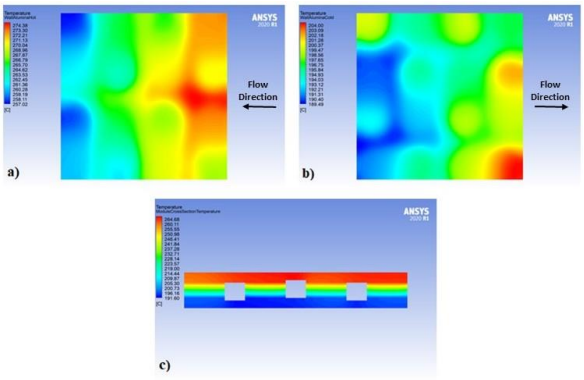

Figure 9. Temperature distributions for 500 °C of T_{hi}: a) on the hot side of the TEM, b) on the cold side of the TEM, and c) through the TEM.

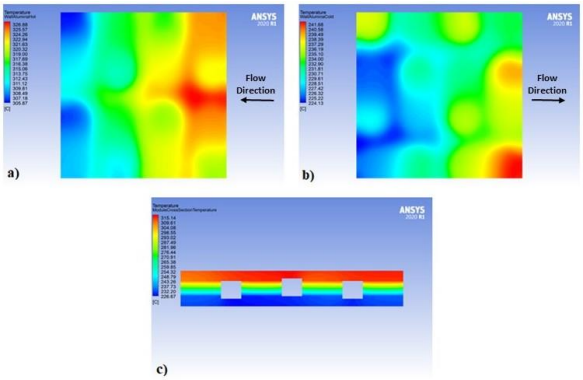

Figure 10. Temperature distributions for 600 °C of T_{hi}: a) on the hot side of the TEM, b) on the cold side of the TEM, and c) through the TEM.

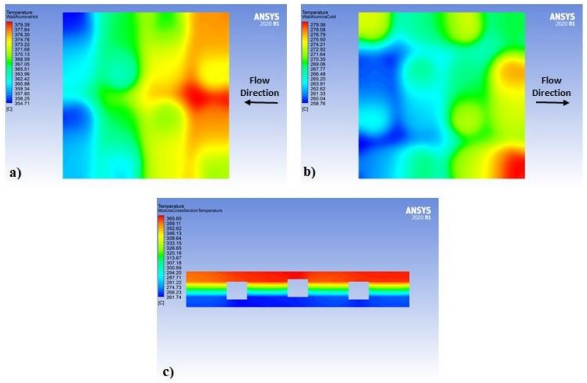

Figure 11. Temperature distributions for 700 °C of T_{hi}: a) on the hot side of the TEM, b) on the cold side of the TEM, and c) through the TEM.

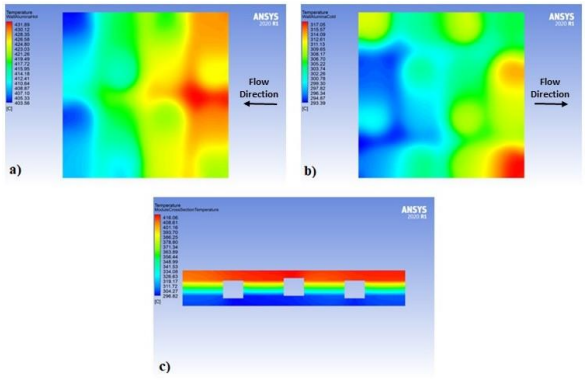

Figure 12. Temperature distributions for 800 °C of T_{hi}: a) on the hot side of the TEM, b) on the cold side of the TEM, and c) through the TEM.

According to the temperature distributions, it has been analyzed that the ΔT of the TEM increase with the increase of the T_{hi}. This increase results in ΔT of 55.6 °C, 70.4 °C, 85.2 °C, 100.1 °C, and 115.0 °C for 400 °C, 500 °C, 600 °C, 700 °C, and 800 °C of T_{hi}, respectively, under constant V_{hi}. The TEM's T_{hs} and T_{cs} for the T_{hi} are given in **Figure 13**. When the temperature distributions are further investigated, it seems that temperature distributions on both sides of the TEM are not homogeneous. The temperature differences on the hot side are 13.7 °C, 17.3 °C, 21.0 °C, 24.6 °C, and 28.3 °C, where the temperature differences on the cold side are 11.4 °C, 14.5 °C, 17.5 °C, 20.6 °C, and 23.6 °C for 400 °C, 500 °C, 600 °C, 700 °C, and 800 °C of T_{hi}, respectively. This difference on the same surface originates from the difference between the conduction heat transfer (occurs between the alumina plate and the silver conductor and between the silver conductor and p- and n-type legs) and the convection heat transfer (occurs between the alumina plate and the ambient air and between p- and n-type legs and the ambient air). In addition, the difference in the thermal conductivity values of the TEM materials (silver conductor and p- and n-type legs) constitutes different values for the conduction heat transfer.

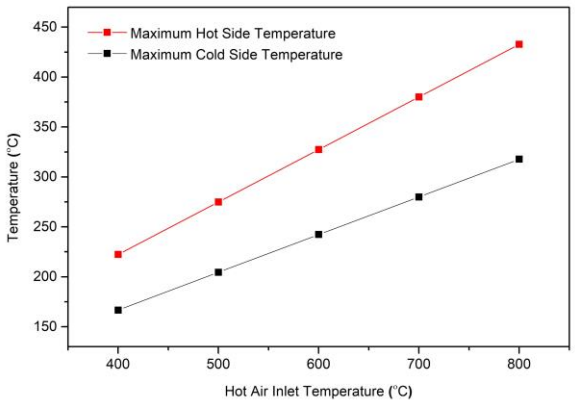

Figure 13. Effect of the T_{hi} on the T_{hs} and T_{cs} of the TEM.

In addition to temperature distributions, the average $\dot{Q}_h$ and $\dot{Q}_c$ of the TEM were investigated. According to the results in **Table 2**, the average $\dot{Q}_h$ of the TEM are found to be 26.7 W, 33.8 W, 40.9 W, 48.0 W, and 55.1 W for 400 °C, 500 °C, 600 °C, 700 °C, and 800 °C of T_{hi}, respectively. In addition, the average $\dot{Q}_c$ of the TEM are analyzed to be 22.2 W, 28.2 W, 34.1 W, 40.0 W, and 45.9 W for 400 °C, 500 °C, 600 °C, 700 °C, and 800 °C of T_{hi}, respectively. According to these results, increasing the T_{hi} yields an increase in $\dot{Q}_h$ and $\dot{Q}_c$ of the TEM. As expected, the maximum average $\dot{Q}_h$ and $\dot{Q}_c$ resulted in the maximum T_{hi}. The increase in $\dot{Q}_h$ and $\dot{Q}_c$ of the TEM can be attributed to the increase in the ΔT between the hot air and the hot side of the TEM, which yields an increase in the convection heat transfer rate.

Table 2. Average $\dot{Q}_h$ and $\dot{Q}_c$ for T_{hi}.

T_{hi} [m/s]	$\dot{Q}_h$ [W]	$\dot{Q}_c$ [W]	T_{hs} [°C]	T_{cs} [°C]	ΔT [°C]
400	26.7	22.2	222.3	166.7	55.6
500	33.8	28.2	274.9	204.5	70.4
600	40.9	34.1	327.5	242.3	85.2
700	48.0	40.0	380.1	280.0	100.1
800	55.1	45.9	432.8	317.8	115.0

IV. CONCLUSIONS

In this study, temperature distributions and $\dot{Q}_h$ and $\dot{Q}_c$ of a TEM were investigated using CFD analyzes. V_{hi} and T_{hi} were altered to specify their effects on T_{hs}, ΔT, and $\dot{Q}_h$. During the analyses, the V_{hi} varied as 1 m/s, 3 m/s, 5 m/s, 10 m/s, and 15 m/s while keeping T_{hi} and T_{ci} at 500 °C and 25 °C, respectively. Afterward, keeping the V_{hi} constant at 15 m/s, and the T_{hi} was modified to 400 °C, 500 °C, 600 °C, 700 °C, and 800 °C.

According to the results, the TEM's maximum T_{hs} and T_{cs} are 274.9 °C and 204.5 °C, respectively. In comparison, the maximum temperature through the TEM is acquired as 266.9 °C for 15 m/s of V_{hi} by keeping the T_{hi} at 500 °C. Increasing the V_{hi} increases

the T_{hs} and T_{cs} and the ΔT of the TEM. This increase derives a ΔT of 70.4 °C for 15 m/s of V_{hi}. In addition to temperature distributions, the average $\dot{Q}_h$ is found to be 33.8 W for 15 m/s of V_{hi}. According to these results, the increase in the T_{hs} and $\dot{Q}_h$ with the increase in V_{hi} can be attributed to the increase in the Re number, which yields an increase in the Nu number and the convection heat transfer coefficient.

When the V_{hi} was kept constant at 15 m/s, the TEM's maximum T_{hs} and T_{cs} were specified as 432.8 °C and 317.8 °C. In contrast, the maximum temperature through the TEM is 419.8 °C for 800 °C of T_{hi}. Increasing the T_{hi} yields an increase in the T_{hs} and T_{cs} and ΔT of the TEM. This increase derives a ΔT of 115.0 °C for 800 °C T_{hi}. In addition to temperature distributions, the average $\dot{Q}_h$ is 55.1 W for 800 °C of T_{hi}. According to these results, the increase in the T_{hs} and $\dot{Q}_h$ with the increase in the T_{hi} can be attributed to the increase in the temperature difference between the hot air and the hot side of the TEM, which yields an increase in the convection heat transfer rate.

ACKNOWLEDGMENTS

This work was supported by the Scientific and Technological Research Council of Turkey (TUBITAK) [grant number 120R009]. Concurrent studies were carried out within the Scientific Research Projects Coordinatorship of Karabuk University [grant number KBÜBAP-21-YL-052].

REFERENCES

[1] Chein, R., Huang, G. Thermoelectric cooler application in electronic cooling. ***Applied Thermal Engineering***, 24 (14–15), 2207–2217 (2004).

[2] Riffat, S. B., Ma, X. Thermoelectrics: A review of present and potential applications. ***Applied Thermal Engineering***, 23 (8), 913–935 (2003).

[3] Xu, X., Dessel, S. V., Messac, A. Study of the performance of thermoelectric modules for use in active building envelopes. ***Building and Environment***, 42 (3), 1489–1502 (2007).

[4] Rowe, D. M., Min, G. Evaluation of thermoelectric modules for power generation. ***Journal of Power Sources***, 73 (2), 193–198 (1998).

[5] Hsiao, Y. Y., Chang, W. C., Chen, S. L. A mathematic model of thermoelectric module with applications on waste heat recovery from automobile engine. ***Energy***, 35 (3), 1447–1454 (2010).

[6] Champier, D., Bedecarrats, J. P., Rivaletto, M., Strub, F. Thermoelectric power generation from biomass cook stoves. ***Energy***, 35 (2), 935–942 (2010).

[7] Ploteau, J. P., Glouannec, P., Noel, H. Conception of thermoelectric flux meters for infrared radiation measurements in industrial furnaces. ***Applied Thermal Engineering***, 27 (2–3), 674–681 (2007).

[8] Chen, W. H., Wang, C. M., Huat Saw, L., Hoang, A. T., Bandala, A. A. Performance evaluation and improvement of thermoelectric generators (TEG): Fin installation and compromise optimization. ***Energy Conversion and Management***, 250, 114858 (2021).

[9] Martínez, A., Astrain, D., Rodríguez, A. Dynamic model for simulation of thermoelectric self-cooling applications. ***Energy***, 55, 1114–1126 (2013).

[10] Bell, L. E. Cooling, Heating, Generating Heat with and Recovering Waste Thermoelectric. ***Science***, 321 (5895), 1457–1461 (2008).

[11] Temizer, I., Ilkiliç, C. The performance and analysis of the thermoelectric generator system used in diesel engines. ***Renewable and Sustainable Energy Reviews***, 63, 141–151 (2016).

[12] He, W., Wang, S., Lu, C., Li, Y., Zhang, X. An optimization analysis of thermoelectric generator structure for different flow directions of working fluids. ***Energy Procedia***, 61, 718–721 (2014).